Molecular Cancer

RESEARCH

Open Access

IFITM3-MET interaction drives osimertinib resistance through AKT pathway activation in *EGFR*-mutant non–small cell lung cancer

Ritsu Ibusuki[1], Eiji Iwama[1*], Atsushi Shimauchi[1], Hiromu Kawano[1], Shun Mizusaki[1], Satoshi Nakamura[1], Yui Miyazaki[1], Yu Inutsuka[1], Mikiko Hashisako[2], Taishi Harada[3], Yuko Tsuchiya-Kawano[4], Hirono Tsutsumi[5], Takayuki Nakanishi[6], Noriaki Nakagaki[7], Yuichiro Koga[8], Shinichi Kimura[9], Shun Mashimoto[10], Daisuke Shibahara[1], Kohei Otsubo[1], Yasuto Yoneshima[1], Kentaro Tanaka[1,11], Yoshinao Oda[2] and Isamu Okamoto[1]

Abstract

Background Despite an initial favorable response of *EGFR*-mutant non–small cell lung cancer (NSCLC) to osimertinib, an EGFR tyrosine kinase inhibitor (TKI), resistance to this drug inevitably develops. Whereas genetic mechanisms for such acquired resistance have been identified, the molecular mediators of resistance induction have remained unclear.

Methods To identify factors that mediate induction of osimertinib resistance, we studied clinical samples from individuals with *EGFR*-mutant NSCLC as well as cell lines including PC-9 and H1975. Methods adopted included transcriptomics analysis and immunohistochemistry of pretreatment NSCLC specimens, spatial transcriptomics analysis, a cell viability assay, immunofluorescence and quantitative PCR analysis, RNA sequencing, immunoblot analysis, comprehensive proteomics analysis by mass spectrometry, co-immunoprecipitation and proximity ligation assays, and a mouse xenograft tumor model.

Results Transcriptomics analysis of pretreatment clinical specimens identified *IFITM3* (interferon-induced transmembrane protein 3) as a gene specifically upregulated in patients with a poor response to osimertinib treatment. Immunohistochemistry confirmed that patients with IFITM3-positive tumors experienced a shorter progression-free survival on osimertinib treatment. Spatial transcriptomics and other analyses further revealed that IFITM3 expression in tumor cells was increased in response to cytokines derived from the tumor microenvironment (TME) during osimertinib treatment. IFITM3 was found to promote the development of osimertinib resistance in NSCLC cell lines through interaction with MET and activation of the AKT signaling pathway. Furthermore, combined treatment with a MET inhibitor suppressed the development of osimertinib resistance in a mouse xenograft tumor model.

*Correspondence:
Eiji Iwama
iwama.eiji.800@m.kyushu-u.ac.jp

Full list of author information is available at the end of the article

Conclusions Our findings reveal that upregulation of IFITM3 driven by TME cytokines represents a previously unrecognized mechanism of osimertinib resistance, and they suggest that targeting of the IFITM3-MET axis may improve EGFR-TKI treatment outcome for *EGFR*-mutant NSCLC.

Keywords IFITM3, Osimertinib, EGFR-TKI, *EGFR*-mutant non–small cell lung cancer, Drug resistance

Introduction

Lung cancer continues to be the leading cause of cancer-related deaths worldwide, with non–small cell lung cancer (NSCLC) being responsible for more than 80% of all lung cancer diagnoses [1]. Mutations of the epidermal growth factor receptor (EGFR) gene are present in ~ 40% of NSCLC cases among Asian populations and in ~ 10% of those among individuals of European descent [2, 3]. Osimertinib, a third-generation EGFR-targeting tyrosine kinase inhibitor (TKI), has shown superior efficacy compared with earlier-generation EGFR-TKIs and has become a standard therapeutic option for patients with *EGFR*-mutated NSCLC [4]. Despite its initial effectiveness, however, the median progression-free survival (PFS) conferred by osimertinib is limited to ~ 19 months, with about one-third of patients developing resistance within a year. Although genetic alterations such as secondary mutations of *EGFR* and amplification of *MET* or *HER2* have been identified as resistance mechanisms [5–8], nearly half of cases do not present identifiable genetic resistance mutations, indicating that nongenetic mechanisms may contribute to such resistance [9].

Recent studies have suggested that the tumor microenvironment (TME) plays a key role in the development of resistance to EGFR-TKIs [10–14]. Specifically, cytokines present within the TME—such as tumor necrosis factor–α (TNF-α), interleukin-6 (IL-6), and interferon-γ (IFN-γ)—have been implicated in the promotion of treatment resistance through modulation of signaling pathways in tumor cells [15–18]. These findings suggest that comprehensive analysis of the TME and tumor cells will be essential to identify key clinical determinants of resistance to osimertinib.

We have now performed RNA–sequencing (seq) analysis of clinical specimens collected from NSCLC patients before osimertinib treatment. We identified *IFITM3* (interferon-induced transmembrane protein 3) as a gene that is specifically upregulated in patients with a poor response to osimertinib treatment. We also investigated the mechanism by which IFITM3 induces resistance to osimertinib and propose that MET inhibition is a potential therapeutic strategy to suppress the development of osimertinib resistance in individuals with NSCLC positive for *EGFR* mutations.

Materials and methods

Patients and clinical specimens

Clinical information, including PFS for osimertinib, was collected for 127 individuals with *EGFR* mutation–positive NSCLC who received osimertinib monotherapy as first-line treatment across eight institutions between January 2016 and April 2023. Formalin-fixed, paraffin-embedded (FFPE) sections of tumor tissue were prepared before osimertinib treatment. In the case of specimens for which RNA-seq analysis was feasible, the analysis was performed for 10 patients with a PFS of < 12 months (short PFS) and 22 patients with a PFS of > 20 months (long PFS). The remaining 95 specimens not subjected to RNA-seq analysis were instead subjected to immunohistochemistry (IHC) for IFITM3, with tumor cells being confirmed by hematoxylin-eosin (HE) staining. At the time of the analysis, 59 of the 95 patients (62.1%) had experienced disease progression during osimertinib treatment. Postprogression tumor specimens were also collected from an additional 18 patients who developed resistance to osimertinib and were subjected to IHC analysis of IFITM3.

RNA-seq analysis of clinical tumor specimens

Tumor tissue was obtained by macrodissection, and RNA was extracted from two FFPE sections (thickness of 10 μm), each with an area of > 1 cm^2, with the use of a MagMAX FFPE DNA/RNA Ultra Kit (#A31881, Thermo Fisher Scientific). Formaldehyde-induced cross-linking was minimized by protease treatment of FFPE sections for 2 h at 55 °C and subsequent incubation for 1 h at 90 °C. RNA-seq analysis was performed with a Twist Human Core Exome Panel (Twist Biosciences). Libraries were prepared from 100 to 200 ng of RNA, depending on the DV200 (percentage of RNA fragments of > 200 nucleotides). Precapture libraries were indexed for Illumina sequencing and amplified for 11 to 16 cycles. Pooled libraries were subjected to hybridization with biotinylated DNA probes for 16 h at 70 °C and were then captured with streptavidin beads (Thermo Fisher Scientific) and amplified to generate postcapture libraries. Quality control was performed with an Agilent Bioanalyzer, and libraries were normalized to a concentration of 2 nM before sequencing. RNA sequencing was conducted with

a NovaSeq instrument (Illumina) and with paired-end reads. All sequencing reads were trimmed of low-quality bases and adapters with the use of Fast p (version 0.23.4, Bolger AM), and RNA-seq reads were mapped to the hg38 genome with the use of HISAT2 software (version 2.2.1). Raw counts for each gene were estimated for each sample with FeatureCounts (version 2.0.6). The $\log_2$(fold change) and *P* values were calculated with edgeR (version 4.0, R Bioconductor).

Cell lines and reagents

Five human NSCLC cell lines with *EGFR* activating mutations (PC-9 [ECACC #90071810], HCC827 [ATCC #CRL-2868], H1975 [ATCC #CRL-5908], H1650 [ATCC #CRL-5883], and HCC4006 [ATCC #CRL-2871]) and five human NSCLC cell lines wild type (WT) for *EGFR* (A549 [ATCC #CCL-185], H322 [ECACC #95111734], Calu-3 [ATCC #HTB-55], H1437 [ATCC #CRL-5872], and H1299 [ATCC #CRL-5803]) were studied. The *EGFR* mutation status of each cell line is provided in Supplemental Table 1. PC-9, H1975, H1650, HCC827, HCC4006, H322, H1437, and H1299 cells were cultured in RPMI 1640 medium (Gibco), and A549 and Calu-3 cells were maintained in Dulbecco's modified Eagle's medium (Gibco). Each medium was supplemented with 10% fetal bovine serum and 1% penicillin-streptomycin (Gibco). All cells were maintained under a humidified atmosphere of 5% CO_2 and at 37 °C. Osimertinib (#S7297, Selleck Chemicals), MK-2206 (#S1078, Selleck Chemicals), capmatinib (#S2788, Selleck Chemicals), and methyl-β-cyclodextrin (#S6827, Selleck Chemicals) were dissolved in dimethyl sulfoxide (Fujifilm Wako) and stored at − 20 °C. Infliximab (Mitsubishi Tanabe Pharma, Osaka, Japan) and tocilizumab (Chugai Pharmaceutical, Tokyo, Japan) were stored at − 20 °C. Recombinant human TNF-α (#210-TA-005, R&D Systems), recombinant human IFN-γ (#300-02, Peprotech), and recombinant human IL-6 (#206-IL, R&D Systems) were dissolved in sterile phosphate-buffered saline (PBS) containing 0.1% bovine serum albumin and were stored at − 20 °C.

RNA interference

Cells were transferred to 96-well plates (Greiner Bio-One) and subjected to transient transfection for 24 h with a small interfering RNA (siRNA) specific for IFITM3 (ID s195035, Thermo Fisher Scientific) or a negative control siRNA (ID 4390843, Thermo Fisher Scientific), each mixed with the RNAiMAX reagent (Thermo Fisher Scientific). For establishment of stable IFITM3-depleted PC-9 and H1975 cell lines, a lentiviral vector containing the IFITM3 short hairpin RNA (shRNA) sequence as well as enhanced green fluorescent protein (EGFP) and puromycin resistance genes—pLV[shRNA]-EGFP: T2A: Puro-U6 > hIFITM3 (ID VB900080-7459hfw)—was constructed and packaged by VectorBuilder. A lentiviral vector for a scrambled shRNA—pLV[shRNA]-EGFP/Puro-U6 > Scramble_shRNA (ID VB010000-0009mxc)—was similarly constructed and packaged.

Retrovirus transduction for generation of stable cell lines

Complementary DNA for *IFITM3* was derived from H1975 cells. Corresponding polymerase chain reaction (PCR) amplicons were prepared with the use of PrimeSTAR GXL DNA Polymerase (#R050A, Takara Bio) and specific primers (Supplemental Table 2) and were ligated into the pQCXIP retroviral vector (#639648, Clontech) between the NotI and BamHI sites with the use of an In-Fusion HD Cloning Kit (#639648, Takara Bio). The resulting vector was designated pQCXIP-IFITM3. A vector for Flag-tagged IFITM3 (pQCXIP-Flag-IFITM3) was similarly prepared (Supplemental Table 2). For establishment of cell lines stably expressing IFITM3 or Flag-IFITM3, the pQCXIP-IFITM3 or pQCXIP-Flag-IFITM3 vector (or the corresponding empty vector [EV] as a control) was first introduced into HEK293T cells (ATCC #CRL-1573) with the use of a Retrovirus Packaging Kit Ampho (#6161, Takara Bio) and the Lipofectamine 3000 reagent (Invitrogen). The resulting culture supernatant containing the recombinant retroviruses was then passed through a 0.45-μm filter, and the filtrate was incubated overnight at 4 °C with a Retro-X Concentrator (Clontech) and then centrifuged at 1500 × *g* for 45 min at 4 °C for isolation of virus pellets. PC-9 or H1975 cells were infected with the retroviruses for 24 h in the presence of polybrene (Nacalai Tesque) at 8 μg/ml and were then cultured in growth medium for an additional 24 h before selection by culture in the presence of puromycin (Invitrogen) at 2 μg/ml. The established cell lines were designated PC-9/EV, H1975/EV, PC-9/IFITM3, H1975/IFITM3, and PC-9/Flag-IFITM3 accordingly.

Cell viability assay

Cells (3000 per well) were seeded in a 96-well flat-bottom plate (Greiner Bio-One) and incubated at 37 °C under 5% CO_2 for 24 h before exposure to test agents and incubation for an additional 72 h. Cell Counting Kit 8 (Nacalai Tesque) reagent (10 μl) was then added to each well, the cells were incubated for an additional 2 h, and absorbance at 450 nm was measured with a Multiskan FC instrument (Thermo Fisher Scientific).

Induction of osimertinib resistance in cell lines

For examination of the development of osimertinib resistance, PC-9/EV, PC-9/IFITM3, H1975/EV, and H1975/IFITM3 cells (1.2×10^5 per well) were seeded in six-well plates (Greiner Bio-One) and exposed to increasing concentrations of osimertinib from 10 nM to 1 μM over a

maximum of 30 days, with the drug concentration being increased when the cells had achieved 70% confluence.

Proteomics analysis by LC-MS/MS

Proteomics analysis was performed by label-free quantitation with liquid chromatography and tandem mass spectrometry (LC-MS/MS). Peptides were separated with a NANO HPLC Capillary Column (Nikkyo Technos), with elution performed over 90 min with a gradient of 5% to 95% acetonitrile at 500 nl/min. Samples were analyzed with an Orbitrap Exploris 240 instrument (Thermo Fisher Scientific) via nano–electrospray ionization. The instrument was operated in data-dependent acquisition mode, capturing full-scan MS spectra at a resolution of 60,000. The top 10 peaks were fragmented with a 30% collision energy and 1.6-*m/z* isolation window, with auto–dynamic exclusion. The acquired spectra were analyzed with Proteome Discoverer 3.0 software (Thermo Fisher Scientific). Proteins that were enriched at least fivefold in samples prepared with antibodies to IFITM3 relative to those prepared with control immunoglobulin G (IgG), and with a P value of <0.05, were considered true binding partners of IFITM3.

Immunoblot analysis

Cells were washed with ice-cold PBS and then lysed in RIPA buffer (Thermo Fisher Scientific) containing protease and phosphatase inhibitors (Nacalai Tesque). The lysates were fractionated by SDS-polyacrylamide gel electrophoresis on a 10% gel, and the separated proteins were transferred to a polyvinylidene difluoride membrane. The membrane was incubated overnight at 4 °C with primary antibodies to IFITM3 (#59212), to phospho-EGFR (#3777), to EGFR (#4267), to phospho-ERK1/2 (#4370), to ERK1/2 (#9102), to phospho-AKT (#9271), to AKT (#9272), to the DYKDDDDK Flag tag (#14793), to phospho-MET (#3077), to MET (#8198), to phospho-GSK3β (#9323), to GSK3β (#9315), to phospho-mTOR (#5536), to mTOR (#2983), or to β-actin (#4970), all of which were obtained from Cell Signaling Technology and used at a dilution of 1:1000. The membrane was subsequently incubated for 1 h at room temperature with horseradish peroxidase–conjugated antibodies to rabbit IgG (diluted 1:10,000; #NA9340, Cytiva), after which immune complexes were detected with the use of Pierce ECL Plus Immunoblotting Substrate (Thermo Fisher Scientific) and images were captured with a ChemiDoc Touch MP system (Bio-Rad). Signals in each lane were quantified with Image Lab (Bio-Rad) and compared with the corresponding β-actin signal for normalization. Corresponding blots were derived from the same experiments and were processed in parallel.

Co-immunoprecipitation for LC-MS/MS or immunoblot analysis

Cells were lysed in Pierce IP Lysis Buffer (#87787, Thermo Fisher Scientific), and the lysates were centrifuged at 15,000 × *g* for 15 min at 4 °C. The resulting supernatants were subjected to immunoprecipitation with constant mixing overnight at 4 °C with antibodies to IFITM3 (#59212, Cell Signaling Technology), control rabbit IgG (#2729, Cell Signaling Technology), or antibodies to Flag (#14793, Cell Signaling Technology) as well as with magnetic protein A/G beads (Pierce). The immune complexes were washed with Tris-buffered saline and then suspended in Pierce IgG Elution Buffer, pH 2.0 (#21028, Thermo Fisher Scientific) for proteomics or immunoblot analysis.

IHC for IFITM3

Tumor tissue was fixed in 10% neutral buffered formalin for preparation of FFPE sections. The sections (thickness, 3 μm) were subjected to IHC as previously described [19]. In brief, antigen retrieval was performed with the use of Immunosaver (Nissin EM), and the sections were incubated overnight at 4 °C with a rabbit monoclonal antibody to IFITM3 (#59212, Cell Signaling Technology). Immune complexes were detected with the Histofine Simple Stain MAX-PO (M) reagent (Nichirei Bioscience) and the chromogenic substrate diaminobenzidine (Histofine DAB, Nichirei Bioscience). IFITM3 immunostaining results were based on staining of neoplastic cells and were reported as positive or negative by an experienced pathologist. The IFITM3 IHC score was defined as follows: 0, < 1% IFITM3-positive tumor cells; 1, 1% to 10%; 2, 10% to 50%; and 3, >50%.

RNA-seq analysis of NSCLC cell lines

Total RNA was isolated with the use of an RNeasy Mini Kit (#74016, Qiagen) from PC-9 cells stably expressing IFITM3 or control shRNAs. Three biological replicates were processed for each condition. The quantity and quality of the isolated RNA were determined with the use of a NanoDrop-2000 spectrophotometer (Thermo Fisher Scientific) and a 2200 TapeStation (Agilent Technologies), respectively, and rRNA was removed with an MGI Easy rRNA Depletion Kit (MGI) before library construction with an MGI Easy RNA Directional Library Prep Set (MGI). Sequencing was conducted with a NovaSeq instrument and with 150-bp paired-end reads. All sequencing reads were trimmed of low-quality bases and adapters with the use of Fast p (version 0.23.4), and RNA-seq reads were mapped to the hg38 genome with the use of HISAT2 software (version 2.2.1). Raw counts for each gene were estimated for each sample with FeatureCounts (version 2.0.6). Gene set enrichment analysis (GSEA) was performed with the use of Metascape [20].

Spatial transcriptomics analysis of clinical specimens

Sample processing and clustering annotation methods were as previously described [21]. A total of eight FFPE tumor specimens was analyzed, including four samples collected from two *EGFR*-mutant NSCLC patients before and after osimertinib treatment as well as an additional four pretreatment samples. Spatial transcriptomics analysis was performed with the 10X Genomics Visium HD platform. The FFPE sections were depleted of paraffin, stained with HE, and imaged with an Evident VS200 microscope. RNA quality was assessed on the basis of DV200, ensuring that all samples met a threshold of ≥ 30%. Gene expression libraries were prepared according to the 10X Genomics protocol, checked for quality, and sequenced with the NovaSeq X Plus platform (150-bp paired-end reads). Sequencing data were processed with Space Ranger (v3.0.0) to generate spatial gene expression profiles. Major clustering analysis was performed according to a single-cell RNA-seq–like pipeline with the use of Scanpy, with low-quality cells and genes being filtered out. Batch effects were corrected by Harmony integration. Leiden clustering at a resolution of 0.4 identified 18 clusters, which were classified into epithelial, stromal, and immune cell types on the basis of known marker expression. Subclustering analysis was further conducted within these major cell types, incorporating inferCNVpy to distinguish tumor cells from normal epithelial cells.

RT-qPCR analysis

Total RNA was extracted from cell lines with the use of an RNeasy Mini Kit (Qiagen) and was subjected to reverse transcription (RT) with a PrimeScript RT Reagent Kit (#RR037A, Takara Bio). The resulting cDNA was subjected to quantitative PCR (qPCR) analysis with SYBR Green PCR Master Mix (#4344463, Thermo Fisher Scientific) and specific primers (Supplemental Table 3). Relative expression of *IFITM3* was analyzed with the $2^{-\Delta\Delta Ct}$ method and was normalized by *GAPDH* mRNA abundance.

Immunofluorescence analysis of IFITM3 expression

PC-9 cells were cultured to 70% confluence on 12-mm-diameter coverslips (Matsunami) placed in 24-well plates (Corning). They were fixed for 15 min with 4% paraformaldehyde in PBS, permeabilized for 10 min with 0.3% Triton X-100 in PBS, and incubated overnight at 4 °C with a 1:500 dilution of Alexa Fluor 488–conjugated antibodies to IFITM3. The antibodies to IFITM3 (#59212, Cell Signaling Technology) were conjugated to the fluorescent dye with the use of a FlexAble CoraLite Plus 488 Antibody Labeling Kit for Rabbit IgG (#KFA001, Proteintech). The cells were subsequently incubated overnight at 4℃ with Alexa Fluor 594–conjugated phalloidin (#ab176757, Abcam). Images of IFITM3 and phalloidin signals were obtained with a BZX800 all-in-one fluorescence microscope (Keyence). Optical sectioning images of IFITM3 particles in multiple cells acquired from top to bottom of each cell were combined into a *z*-projection image with the use of full-focus imaging (BZ-H4A, Keyence). The number of IFITM3 signals per cell was quantified in nine fields, including a total of at least 50 cells for each condition, with the use of BZ-X Analyzer software (BZ-H4A, Keyence).

In situ proximity ligation assay (PLA)

PC-9/EV and PC-9/IFITM3 cells were cultured to 70% confluence on 12-mm-diameter coverslips in 24-well plates, fixed, and permeabilized as described in the previous section. They were then incubated overnight at 4 °C with 1:500 dilutions of mouse antibodies to IFITM3 (#2524, Cell Signaling Technology) and rabbit antibodies to MET (#8242, Cell Signaling Technology) for detection of IFITM3-MET complexes with the use of Duolink PLA Fluorescence Kits (#DUO92002 and #DUO92004, Sigma-Aldrich). The cells were subsequently incubated overnight at 4℃ with antibodies to E-cadherin (#AF648, R&D Systems) and for 1 h at room temperature with Alexa Fluor 488–conjugated donkey antibodies to goat IgG (#A11055, Invitrogen). Imaging and analysis of PLA and E-cadherin signals were performed as described in the previous section.

Animal studies

Four-week-old female athymic mice were obtained from CLEA Japan. PC-9/EV or PC-9/IFITM3 cells (5.0×10^6) were injected subcutaneously into the flank of the mice, which were randomly divided into the treatment groups described in Fig. 6 at 7 days after cell injection. Tumor dimensions were measured twice each week, and tumor volume was calculated according to the formula: (length × width × width)/2. Mice were killed by cervical dislocation under anesthesia with a mixture of medetomidine, midazolam, and butorphanol when tumors achieved a volume of >2000 mm^3 or at 28 days after treatment onset.

Statistical analysis

Data are presented as means ± s.e.m. unless indicated otherwise and were compared by Fisher's exact test or by one-way analysis of variance (ANOVA) followed by Tukey's test as performed with GraphPad Prism 10 software. The optimal cutoff for IFITM3 positivity was determined according to model selection criteria, including the Corrected Akaike Information Criterion (AICc) and Bayesian Information Criterion (BIC), with the use of JMP 17 software. Kaplan-Meier analysis and log-rank tests were also performed with JMP 17. A P value of < 0.05 was considered statistically significant.

Results

High IFITM3 expression is associated with poor efficacy of osimertinib treatment for EGFR-mutant NSCLC

We analyzed FFPE tumor sections and clinical data for 127 individuals with *EGFR*-mutant NSCLC who received osimertinib monotherapy as a first-line treatment between January 2016 and April 2023 across eight institutions. We defined short and long PFS as < 12 and >20 months, respectively, on the basis of the results of a previous clinical study of osimertinib treatment [4]. RNA-seq analysis was performed for 32 patients with a short PFS (n = 10) or long PFS (n = 22) who had sufficient RNA available, with these individuals constituting the discovery cohort (Fig. 1a and Supplemental Table 4). The remaining 95 patients constituted the validation cohort, which was analyzed by IHC (Fig. 1a). The RNA-seq analysis was successful for all specimens of the discovery cohort, with a high number of detected genes and high mapping rate (which was >80% in all and >90% in most cases, indicative of the consistently high quality of the data) (Supplemental Fig. 1a). In addition, gene expression patterns were closely aligned among the samples (Supplemental Fig. 1b). Comparison of gene expression between patients with a short versus long PFS identified *IFITM3* as the only significantly upregulated gene among >19,000 genes analyzed (Fig. 1b). Patients with high *IFITM3* expression manifested not only a shorter PFS but also a poorer response rate for osimertinib treatment compared with those with low *IFITM3* expression (Fig. 1c, d). To validate the association between *IFITM3* expression and osimertinib efficacy, we performed IHC analysis for the 95 eligible clinical specimens in the validation cohort (Fig. 1e–h and Supplemental Table 5). We investigated the optimal cutoff for the percentage of IFITM3-positive tumor cells within tissue sections by comparing thresholds of 1%, 10%, and 50% with model selection criteria (AICc and BIC), with this analysis indicating that 10% was the best-fitting cutoff (Supplemental Table 6). Patients with IFITM3-positive tumors experienced a significantly shorter PFS relative to those with IFITM3-negative tumors (median of 18.4 vs. 24.8 months; hazard ratio [HR] of 1.87, with a 95% confidence interval [CI] of 1.06–3.30; P = 0.013) (Fig. 1f).

IFITM3 expression is associated with osimertinib resistance in EGFR-mutant NSCLC cell lines

Immunoblot analysis revealed that the abundance of IFITM3 was higher in NSCLC cell lines harboring *EGFR* driver mutations (L858R point mutation or exon-19 deletions) than in those WT for *EGFR* (Fig. 2a). Analysis of public data for 1156 solid tumor cell lines in the Cancer Cell Line Encyclopedia (CCLE) [22] also revealed that *IFITM3* mRNA abundance was significantly higher in cell lines with *EGFR* driver mutations than in those WT for *EGFR* or with other *EGFR* mutations (Fig. 2b). We also analyzed transcriptomics data for clinical samples of advanced-stage lung adenocarcinoma in the The Cancer Genome Atlas (TCGA) cohort stratified by *EGFR* genotype. Consistent with the cell line results, tumors with *EGFR* driver mutations showed significantly higher *IFITM3* expression compared with those WT for *EGFR* (Fig. 2c). These results suggested that IFITM3 expression is closely associated with EGFR signaling, and that targeting of IFITM3 is potentially more important for tumors with *EGFR* driver mutations. We therefore investigated the role of IFITM3 in osimertinib resistance in such *EGFR*-mutated NSCLC cell lines. We subjected five *EGFR*-mutant NSCLC cell lines to siRNA-mediated knockdown of IFITM3. Combined IFITM3 knockdown and osimertinib exposure resulted in a significantly greater loss of cell viability compared with either treatment alone (Fig. 2d). Consistent with these findings, stable knockdown of IFITM3 with a specific shRNA increased sensitivity of the cell lines to osimertinib (Fig. 2e, f), whereas forced expression of IFITM3 reduced osimertinib sensitivity (Fig. 2g, h). Long-term exposure to osimertinib revealed that cells overexpressing IFITM3 developed resistance to 1 μM osimertinib within 30 days of treatment, whereas control cells did not manifest such resistance (Fig. 2i, j).

IFITM3 expression increases after osimertinib treatment

We previously performed a spatial transcriptomics analysis for clinical specimens of *EGFR*-mutant NSCLC collected before osimertinib treatment and after the development of drug resistance [21]. Using this data set, we analyzed *IFITM3* expression and its potential modulators within the TME for two patients: one who developed resistance to osimertinib treatment with a short PFS of 6 months, and one showing prolonged drug efficacy with a long PFS of 36 months. Transcriptional and histological (HE staining) analyses identified distinct cell clusters including those corresponding to tumor cells, macrophages, fibroblasts, T cells, and B cells (Fig. 3a). Tumor cells showed the highest *IFITM3* expression among all cell clusters (Fig. 3b). For the pretreatment specimens, *IFITM3* expression in tumor cells was significantly higher for the patient with the short PFS than for the patient with the long PFS (Fig. 3a, c), consistent with our RNA-seq and IHC findings. Of note, *IFITM3* expression was increased in the posttreatment specimens compared with the pretreatment specimens for both patients (Fig. 3a, c). Comparison of IFITM3 protein expression between the 95 pretreatment specimens of the validation cohort (Fig. 1a) and an additional 18 posttreatment specimens

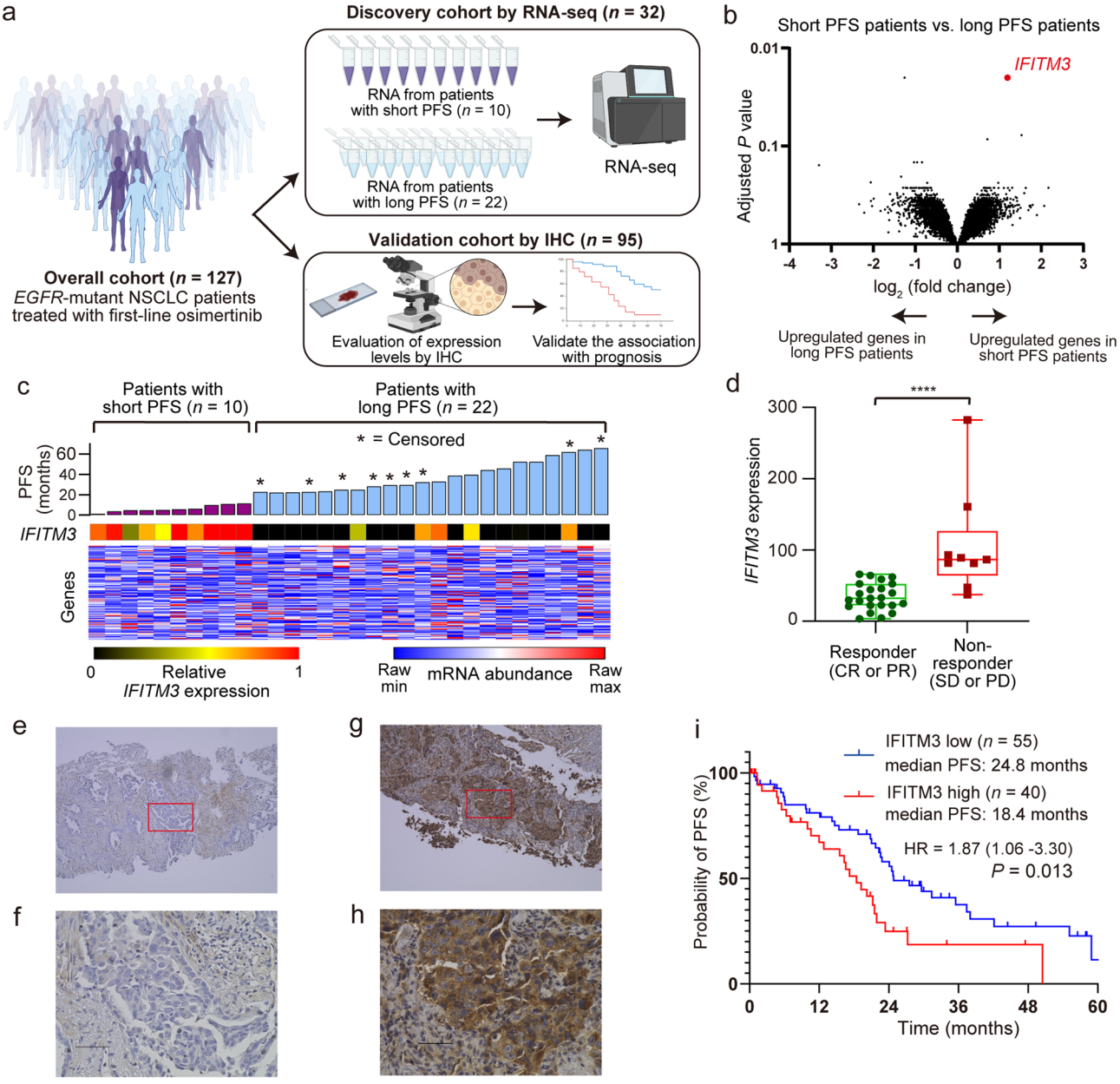

Fig. 1 IFITM3 expression is associated with poor clinical outcomes in *EGFR*-mutant NSCLC. **a** Experimental design. The overall cohort of *EGFR*-mutated NSCLC patients who received first-line osimertinib treatment ($n = 127$) was divided into a discovery cohort ($n = 32$) subjected to RNA-seq analysis and a validation cohort ($n = 95$) subjected to IHC analysis. In the discovery cohort, patients with a short PFS (< 12 months, $n = 10$) were compared with those with a long PFS (> 20 months, $n = 22$). **b** Volcano plot of differences in gene expression for patients with a short PFS versus those with a long PFS. The red dot in the upper right quadrant indicates an upregulated gene in patients with a short PFS (adjusted *P* value of < 0.05, $\log_2$(fold change) of > 1). **c** Heat maps of *IFITM3* and other gene expression levels for the 32 patients in the discovery cohort arranged from left to right in ascending order of PFS. PFS is shown as a bar graph, with asterisks indicating censored patients. **d** *IFITM3* mRNA abundance according to treatment response in the discovery cohort. Responders were defined as patients who showed a complete response (CR) or partial response (PR), and nonresponders as those showing stable disease (SD) or progressive disease (PD). ****$P < 0.0001$ (one-way ANOVA followed by Tukey's test). **e**–**h**, Representative low (**e**-**g**) and high (**f**-**h**) magnification images for IHC analysis of IFITM3 in tumor specimens with low (**e**-**f**) or high (**g**-**h**) IFITM3 expression. Scale bars, 50 μm. **i**, Kaplan-Meier plot for PFS according to IFITM3 expression status for the validation cohort

revealed that the abundance of IFITM3 was significantly higher in the latter specimens (Supplemental Fig. 2a). Together, these findings suggested that osimertinib treatment induces IFITM3 expression in tumor cells.

Osimertinib induces IFITM3 expression in a cytokine-dependent manner

Given that IFITM3 expression has been shown to be upregulated by various cytokines [23, 24], we examined

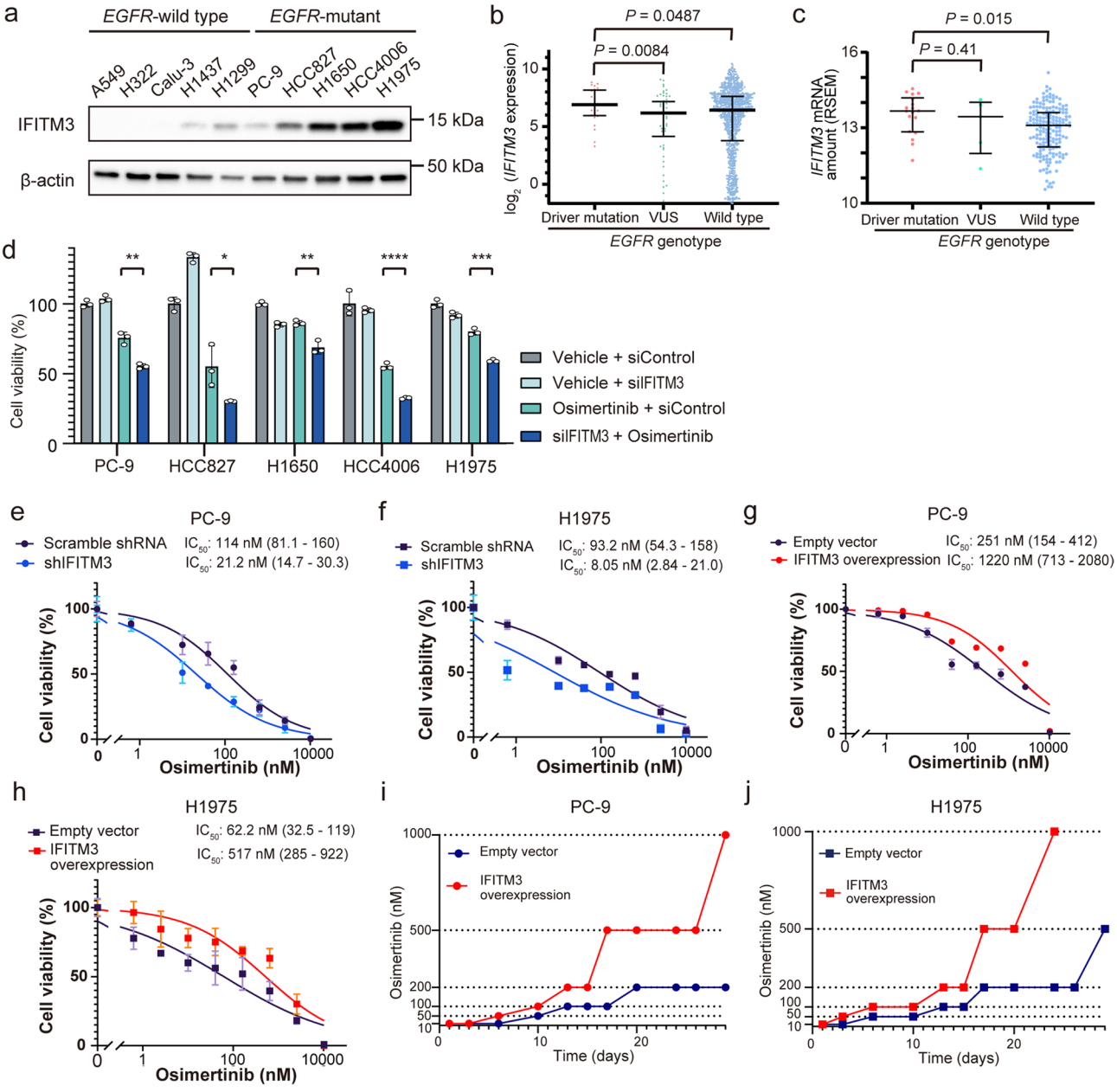

Fig. 2 IFITM3 expression reduces osimertinib sensitivity and induces osimertinib resistance. **a** Immunoblot analysis of IFITM3 and β-actin (loading control) in human *EGFR*-WT and *EGFR*-mutant NSCLC cell lines. **b**,**c**, *IFITM3* mRNA abundance according to *EGFR* genotype for 1156 solid tumor cell lines in the CCLE database (**b**) and for 199 stage III or IV lung adenocarcinoma patients in the TCGA database (**c**). VUS, variant of uncertain significance; RSEM, RNA-seq by Expectation-Maximization. Bars indicate the median and 95% CI. The *P* values were determined with one-way ANOVA followed by Tukey's test. **d**, Colorimetric viability assay for *EGFR*-mutant NSCLC cell lines transfected with control or IFITM3 siRNAs and exposed to 100 nM osimertinib or vehicle for 72 h. **P* < 0.05, ***P* < 0.01, ****P* < 0.001, *****P* < 0.0001 (one-way ANOVA followed by Tukey's test). **e**-**f**, Viability assay for PC-9 (**e**) and H1975 (**f**) cells stably transduced with IFITM3 or scrambled shRNAs and exposed to the indicated concentrations of osimertinib for 72 h. **g**-**h**, Viability assay for PC-9 (**g**) and H1975 (**h**) cells stably overexpressing IFITM3 or harboring the corresponding empty vector and exposed to the indicated concentrations of osimertinib for 72 h. **i**-**j** Time course for the development of osimertinib resistance in PC-9 (**i**) and H1975 (**j**) cells stably overexpressing IFITM3 or harboring the corresponding empty vector. The concentration of osimertinib was gradually increased from 10 nM to 1 μM each time the cells achieved 70% confluence. Osimertinib concentration increments are indicated on the *y*-axis. Data in **d** to **h** are means ± s.e.m. of triplicates from one experiment and are representative of three independent experiments. Median inhibitory concentration (IC_{50}) values with the 95% CI are indicated in **e** to **h**. Data in **i** and **j** are for one of two independent experiments, each conducted without replicates

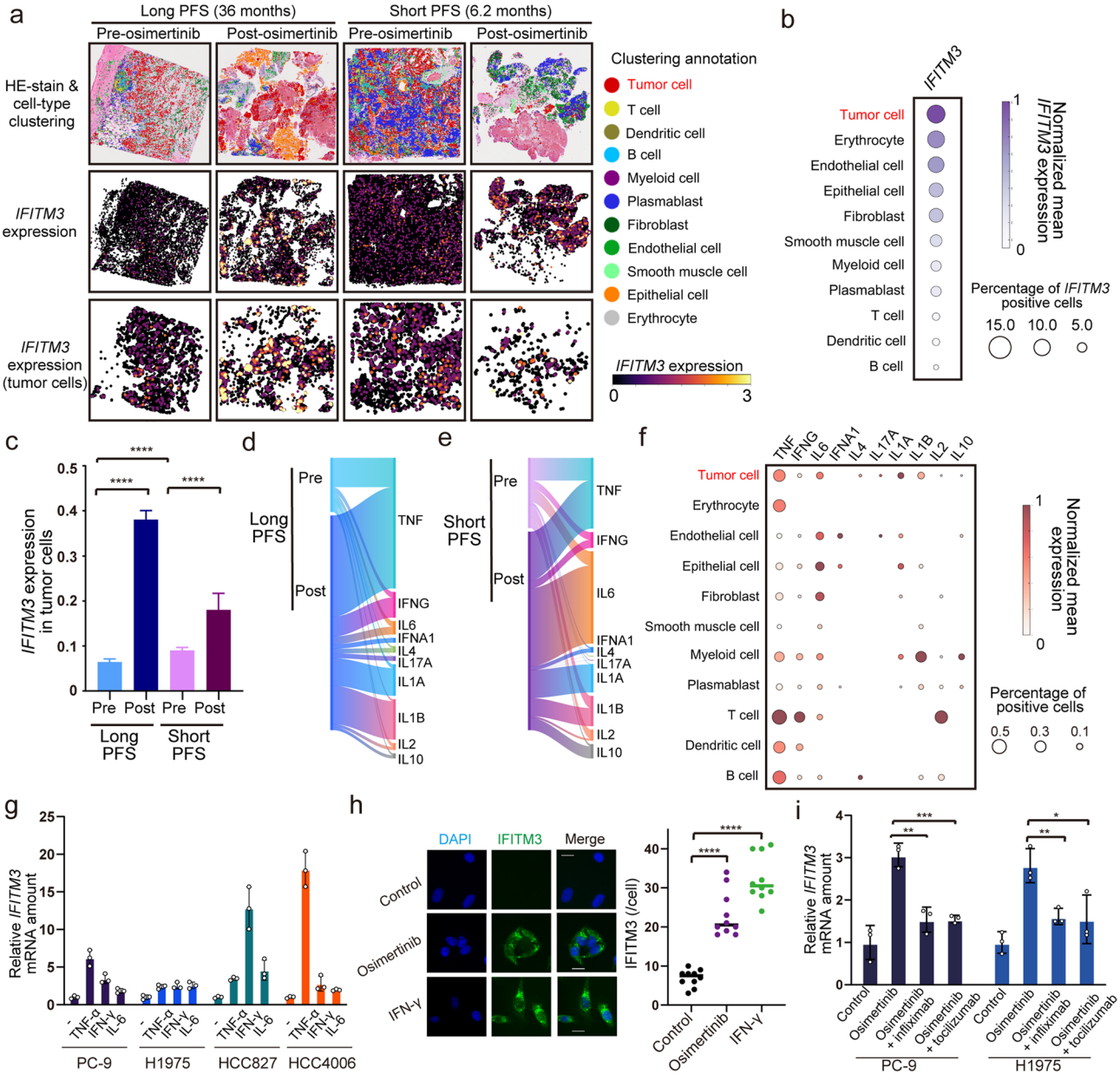

Fig. 3 IFITM3 expression is upregulated by cytokines released in the TME in response to osimertinib treatment. **a**–**f**, Spatial transcriptomics analysis of tumor specimens obtained before and after osimertinib treatment for two *EGFR*-mutated NSCLC patients, one with a long and one with a short PFS [21]. **a** HE staining and clustering analysis (upper panels), *IFITM3* expression in all cells (middle panels), and *IFITM3* expression in tumor cells (lower panels). **b** *IFITM3* expression and the number of cells positive for such expression according to cell type. **c**, *IFITM3* expression in tumor cells before and after the development of osimertinib resistance for the two patients with a long or short PFS. Bars indicate the median and 95% CI. **d**-**e**, Sankey diagrams showing expression of cytokine genes in cells surrounding tumor cells before and after osimertinib treatment for the two patients with a long (**d**) or short (**e**) PFS. **f**, Bubble plot showing the expression levels of cytokine genes and the corresponding number of positive cells for each cell type among all cells. **g** RT-qPCR analysis of *IFITM3* mRNA abundance in *EGFR*-mutant NSCLC cell lines incubated in the absence or presence of TNF-α (10 ng/ml), IL-6 (10 ng/ml), or IFN-γ (50 ng/ml) for 24 h. **h** Immunofluorescence analysis of IFITM3 (green) in PC-9 cells incubated in the absence or presence of osimertinib (100 nM) or IFN-γ (50 ng/ml) for 24 h. Nuclei were stained with 4′,6-diamidino-2-phenylindole (DAPI, blue). The representative images were obtained by optical sectioning. Scale bars, 20 μm. The number of IFITM3 fluorescent particles per cell was also determined ($n = 9$ fields including a total of at least 50 cells). Bars indicate median values. **i**, RT-qPCR analysis of *IFITM3* mRNA abundance in PC-9 and H1975 cells incubated with or without osimertinib (100 nM) and antibodies to TNF-α (infliximab, 1 μg/ml) or to IL-6R (tocilizumab, 10 μg/ml) for 24 h. Data in **g** and **i** are means ± s.e.m. for triplicates from one experiment and are representative of two independent experiments. *$P < 0.05$, **$P < 0.01$, ***$P < 0.001$, ****$P < 0.0001$ (one-way ANOVA followed by Tukey's test)

the expression of cytokine genes in cells surrounding tumor cells using the spatial transcriptomics data for the clinical specimens. The expression of inflammatory cytokine genes including those for TNF-α, IL-6, and IFN-γ was markedly elevated in the posttreatment samples compared with the pretreatment samples for both patients (Fig. 3d, e). Furthermore, the expression of these cytokine genes in cells around tumor cells was higher in the pretreatment specimen from the patient with the short PFS than in that from the patient with the long PFS (Supplemental Fig. 2b). Although these cytokine genes were found to be expressed predominantly by TME cells, they were also expressed in tumor cells (Fig. 3f). RT-qPCR analysis confirmed that treatment with TNF-α, IL-6, or IFN-γ or with osimertinib indeed increased *IFITM3* expression in *EGFR*-mutant NSCLC cell lines (Fig. 3g and Supplemental Fig. 3a). Immunofluorescence analysis similarly showed that IFITM3 protein abundance in PC-9 cells was upregulated in response to osimertinib treatment or cytokine stimulation (Fig. 3h), and that a fraction of the protein was localized to the cell membrane (Supplemental Fig. 3b). Treatment with antibodies to the IL-6 receptor (IL-6R) or to TNF-α suppressed the osimertinib-induced increase in *IFITM3* expression in NSCLC cell lines (Fig. 3i), indicating that this effect of osimertinib was dependent on cytokines derived from the tumor cells. To investigate possible differences in cell types surrounding tumor cells with or without *IFITM3* expression, we performed spatial transcriptomics analysis for a total of eight samples including an additional four pretreatment samples as well as the four previously analyzed samples (Supplemental Fig. 4a). *IFITM3* expression in tumor cells was heterogeneous across the specimens (Fig. 3a and Supplemental Fig. 4a), with a total of 14,698 IFITM3-positive cells and 112,490 IFITM3-negative cells. We analyzed cell type for the 50 cells closest to each tumor cell and found no significant differences in the proportions of TME cell types according to the absence or presence of *IFITM3* expression in the tumor cells (Supplemental Fig. 4b).

Osimertinib resistance mediated by IFITM3 is associated with activation of the PI3K-AKT signaling pathway

To elucidate the mechanism by which IFITM3 reduces the sensitivity of tumor cells to osimertinib, we performed RNA-seq analysis of PC-9 cells stably depleted of IFITM3 with a specific shRNA and corresponding control cells. Knockdown of IFITM3 resulted in downregulation of tumor-promoting genes such as *TOP2A* and *MKI67* (Fig. 4a). GSEA further revealed that depletion of IFITM3 induced significant downregulation of genes associated with poor survival in lung cancer (Fig. 4b). Kyoto Encyclopedia of Genes and Genomes (KEGG) pathway enrichment analysis also revealed significant changes in the expression of cancer-related genes, with the phosphatidylinositol 3-kinase (PI3K)–AKT signaling pathway being markedly affected (Fig. 4c). Consistent with this result, immunoblot analysis showed that the phosphorylation level of AKT was increased by stable overexpression of IFITM3 in *EGFR*-mutant cell lines even in the presence of osimertinib (Fig. 4d and Supplemental Fig. 5a). Conversely, siRNA-mediated knockdown of IFITM3 reduced AKT phosphorylation, resulting in a decreased phosphorylation level for glycogen synthase kinase 3β (GSK3β), a downstream effector of AKT signaling (Fig. 4e and Supplemental Fig. 5b–d). Moreover, whereas treatment with the AKT inhibitor MK-2206 alone had little effect on cell viability (Supplemental Fig. 6), this agent restored osimertinib sensitivity in cells stably overexpressing IFITM3 (Fig. 4f, g). These findings indicated that IFITM3-mediated osimertinib resistance is driven by activation of the PI3K-AKT signaling pathway.

IFITM3 induces osimertinib resistance through activation of MET-AKT signaling

To investigate the mechanism by which IFITM3 activates the PI3K-AKT pathway, we performed co-immunoprecipitation analysis of two *EGFR*-mutant NSCLC cell lines (PC-9 and H1975) with antibodies to IFITM3. The IFITM3 binding proteins in the immunoprecipitates were subjected to comprehensive proteomics analysis by LC-MS/MS. A total of 546 and 253 proteins were identified as candidate IFITM3 binding proteins in PC-9 and H1975 cells, respectively, with 97 proteins being shared between the two cell lines (Fig. 5a). Fifty-eight of these 97 shared proteins were found to be membrane proteins (Supplemental Fig. 7), with the receptor tyrosine kinase MET being the only protein associated with the PI3K-AKT pathway (Fig. 5a and Supplemental Table 7). Co-immunoprecipitation analysis with antibodies to the Flag epitope tag for PC-9 cells stably expressing Flag-tagged IFITM3 confirmed the binding of IFITM3 to MET (Fig. 5b). A PLA revealed a significant increase in the number of IFITM3-MET complexes in cells stably overexpressing IFITM3 compared with control cells (Fig. 5c, d). Immunoblot analysis also showed that stable IFITM3 knockdown in PC-9 cells was associated with a reduced level of MET phosphorylation as well as of AKT phosphorylation (Fig. 5e and Supplemental Fig. 5e). These findings thus suggested that IFITM3 induces activation of AKT signaling by binding to MET. We next assessed the efficacy of MET inhibition in NSCLC cell lines stably expressing IFITM3. Whereas treatment with the MET inhibitor capmatinib alone had little effect on cell viability (Supplemental Fig. 8), this agent restored sensitivity to osimertinib in the cells stably overexpressing IFITM3 (Fig. 5f, g). In addition, given that IFITM3 has been shown to stabilize lipid rafts [25], we investigated

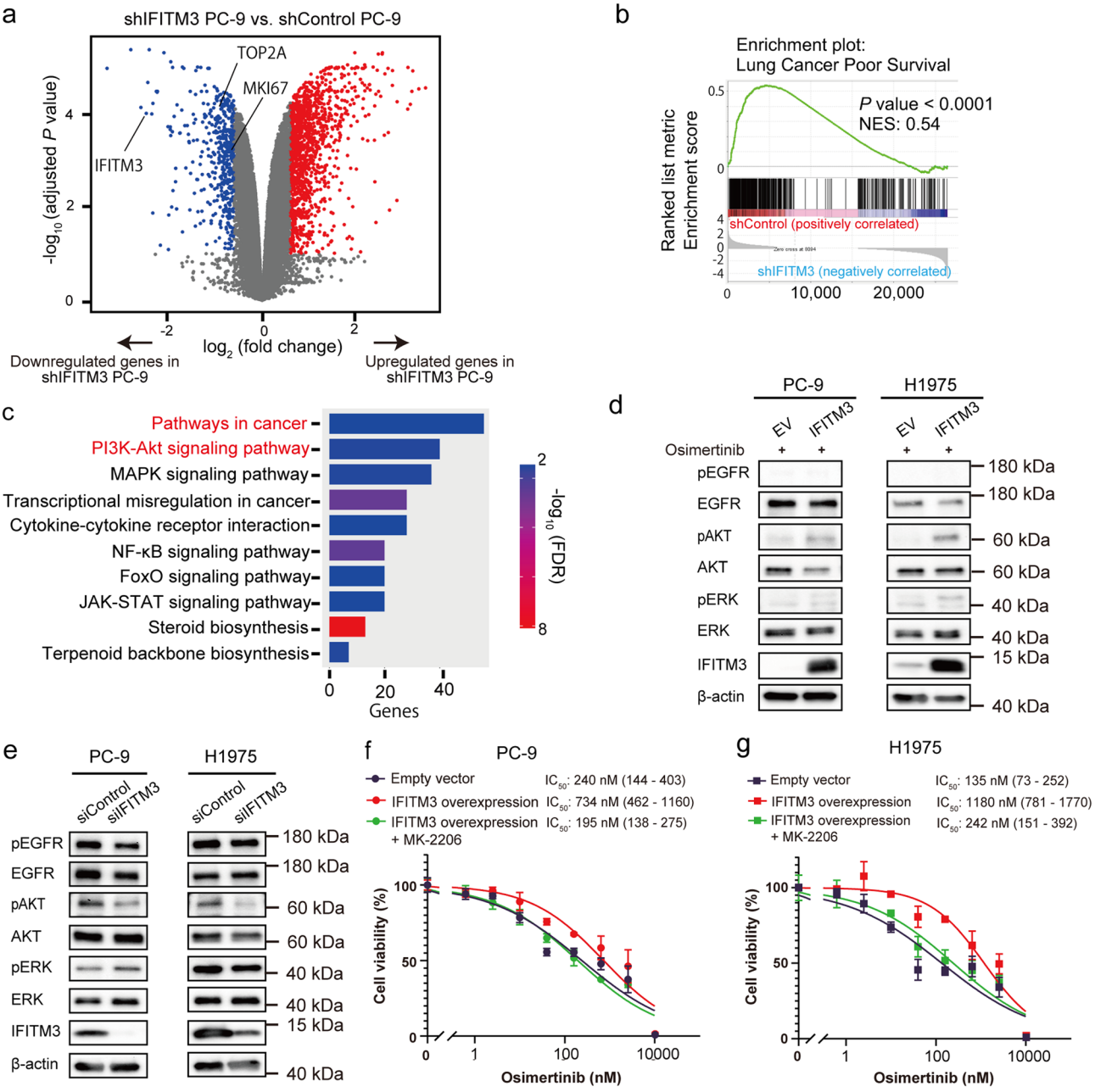

Fig. 4 IFITM3 reduces osimertinib sensitivity via PI3K-AKT pathway activation. **a** Volcano plot for differences in gene expression revealed by RNA-seq analysis of PC-9 cells stably expressing IFITM3 shRNA or a control shRNA ($n = 3$ biological replicates). The red and blue dots indicate upregulated and downregulated genes, respectively, in the IFITM3-depleted cells (adjusted P value of < 0.05, $\log_2$(fold change) of > 1 or < -1). **b** GSEA of the RNA-seq data for the Lung Cancer Poor Survival gene set. NES, normalized enrichment score. **c**, KEGG pathway analysis for the downregulated differentially expressed genes identified in the RNA-seq analysis. Pathways are ranked by the number of associated genes and are color-coded according to the $-\log_{10}$(false discovery rate [FDR]) values. **d** Immunoblot analysis of total or phosphorylated (p) forms of EGFR, AKT, ERK, and IFITM3 in PC-9 and H1975 cells stably overexpressing IFITM3 or harboring the corresponding empty vector (EV) and exposed to 100 nM osimertinib for 24 h. **e** Immunoblot analysis of total or phosphorylated (p) forms of EGFR, AKT, ERK, and IFITM3 in PC-9 and H1975 cells expressing control or IFITM3 siRNAs in the absence of osimertinib. **f**-**g** Viability assay for PC-9/IFITM3 and PC-9/EV cells (**f**) or for H1975/IFITM3 and H1975/EV cells (**g**) treated with the indicated concentrations of osimertinib in the absence or presence of MK-2206 (500 nM) for 72 h. Data in **f** and **g** are means ± s.e.m. for triplicates from one experiment and are representative of three independent experiments. IC_{50} values with the 95% CI are also indicated

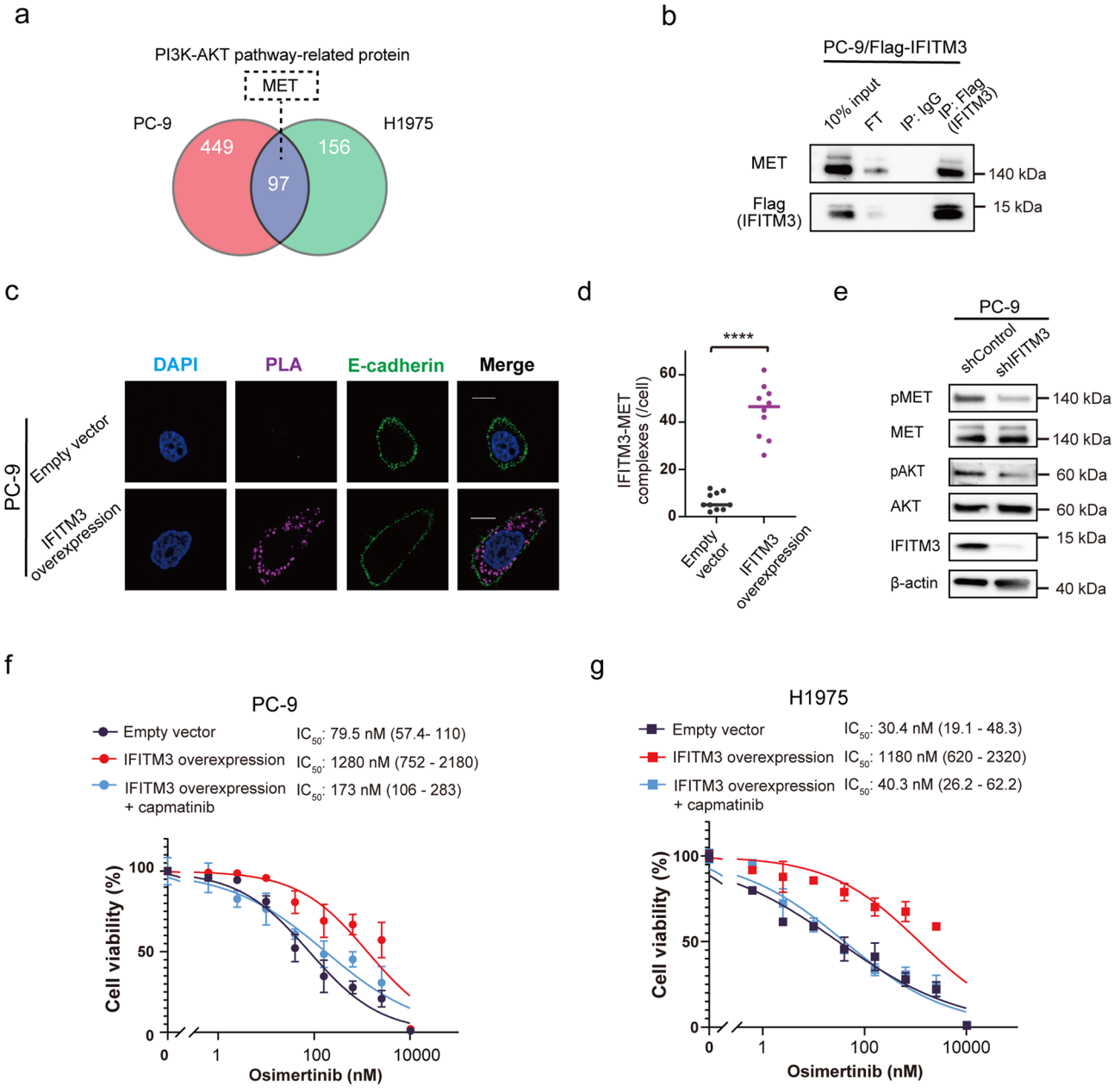

Fig. 5 IFITM3 activates the AKT pathway by interacting with MET. **a** Venn diagram showing the overlap in the number of proteins identified as potential IFITM3 binding proteins by LC-MS/MS analysis of immunoprecipitates prepared from PC-9 and H1975 cells with antibodies to IFITM3. **b** Co-immunoprecipitation analysis with antibodies to Flag (or control IgG) for PC-9 cells stably expressing Flag-tagged IFITM3. The immunoprecipitates (IP), as well as the original cell lysates (10% input) and the flow-through (FT) solution of IP samples, were subjected to immunoblot analysis with antibodies to MET and to Flag. **c** Fluorescence microscopic images of IFITM3-MET complexes (purple) detected by an in situ PLA for PC-9/EV and PC-9/IFITM3 cells. The cells were also stained with antibodies to E-cadherin (green) and with DAPI (blue). The representative images were obtained by optical sectioning. Scale bars, 10 μm. **d** The number of IFITM3-MET complexes per cell was determined as in **c** ($n = 10$ fields including a total of at least 50 cells). Bars indicate median values. ****$P < 0.0001$ (one-way ANOVA followed by Tukey's test). **e** Immunoblot analysis of total or phosphorylated (p) forms of MET, AKT, and IFITM3 in PC-9 cells expressing IFITM3 or control shRNAs. **f**-**g**, Viability assay for PC-9/EV and PC-9/IFITM3 cells (**f**) or for H1975/EV and H1975/IFITM3 cells (**g**) treated with the indicated concentrations of osimertinib in the absence or presence of capmatinib (100 nM) for 72 h. Data in **f** and **g** are means ± s.e.m. for triplicates from one experiment and are representative of three independent experiments. IC_{50} values with the 95% CI are also indicated

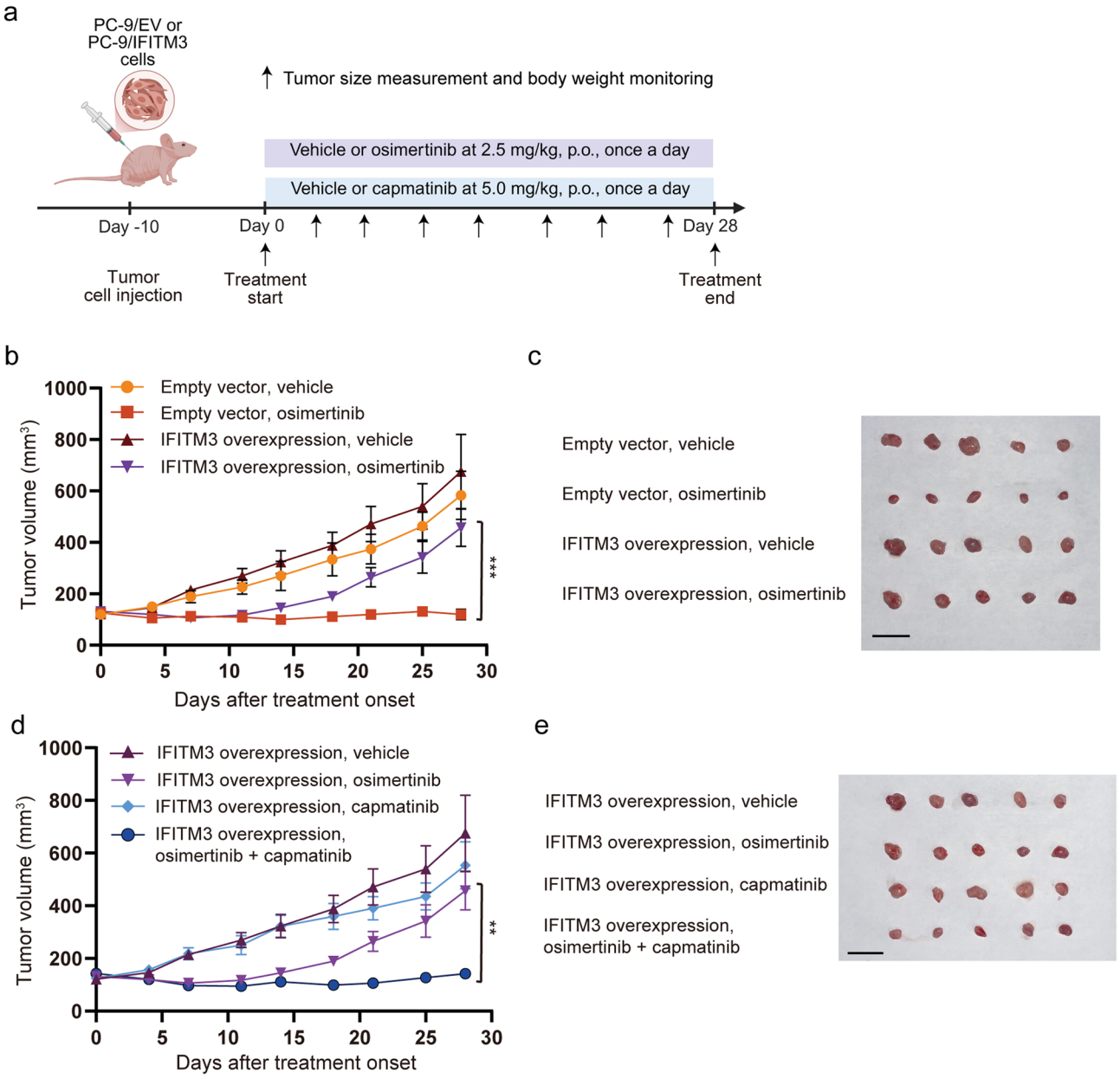

Fig. 6 A MET inhibitor suppresses the development of IFITM3-dependent osimertinib resistance in a xenograft mouse model. **a** Treatment protocol for the xenograft mouse model. PC-9/EV or PC-9/IFITM3 cells were injected into the flank of nude mice at day − 10. Treatment by daily oral administration of vehicle or osimertinib (2.5 mg/kg) or of vehicle or capmatinib (5.0 mg/kg) was initiated on day 0. The mice were killed on day 28. **b** Time course of tumor volume for subcutaneous tumors formed by PC-9/EV or PC-9/IFITM3 cells in nude mice treated with vehicle or osimertinib from day 0. **c** Tumors isolated from mice in **b** at day 28. Scale bar, 20 mm. **d** Time course of tumor volume for subcutaneous tumors formed by PC-9/IFITM3 cells in nude mice treated with vehicle, osimertinib, or capmatinib as indicated from day 0. **e** Tumors isolated from mice in **d** at day 28. Scale bar, 20 mm. All quantitative data are means ± s.e.m. ($n = 5$ mice per group). $^{**}P < 0.01$, $^{***}P < 0.001$ (one-way ANOVA followed by Tukey's test)

the potential contribution of lipid rafts to IFITM3-mediated MET pathway activation. Treatment with a lipid raft inhibitor, methyl-β-cyclodextrin, reversed the IFITM3-induced increase in MET phosphorylation (Supplemental Fig. 9a, b) as well as restored sensitivity to osimertinib (Supplemental Fig. 9c) in IFITM3-overexpressing cells, whereas treatment with MβCD alone had little effect on cell viability (Supplemental Fig. 9d), suggesting that IFITM3-mediated MET pathway activation is facilitated by lipid rafts.

MET Inhibition suppresses the development of IFITM3-mediated osimertinib resistance in a xenograft mouse model

To further validate our findings in vivo, we established a xenograft mouse model by subcutaneously injecting

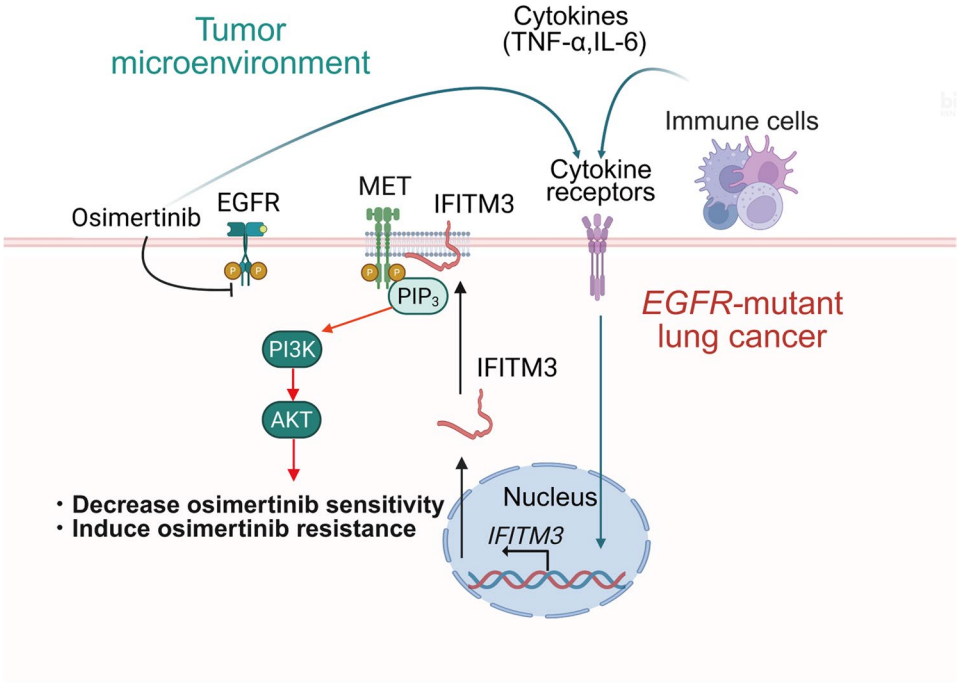

Fig. 7 Proposed mechanism for the development of IFITM3-mediated osimertinib resistance in *EGFR* mutation–positive NSCLC. Cytokines produced by immune and nonimmune cells of the TME induce IFITM3 expression in *EGFR*-mutant lung cancer cells in response to osimertinib treatment. Osimertinib also induces cytokine production in cancer cells themselves, further increasing IFITM3 expression. IFITM3 interacts with MET and thereby activates the PI3K-AKT pathway, resulting in reduced sensitivity to osimertinib and the development of osimertinib resistance. PIP_3, phosphatidylinositol 3,4,5-trisphosphate

PC-9 cells stably overexpressing IFITM3 (PC-9/IFITM3 cells) into athymic nude mice (Fig. 6a). Whereas tumors derived from PC-9 cells harboring the empty vector (PC-9/EV cells) responded well to osimertinib treatment, those formed by PC-9/IFITM3 cells rapidly developed resistance to osimertinib (Fig. 6b, c). However, this rapid tumor growth manifested by PC-9/IFITM3 cells treated with osimertinib was effectively inhibited by concurrent treatment with capmatinib (Fig. 6d, e), with no mice experiencing weight loss of ≥ 10% (Supplemental Fig. 10). These findings indicated that MET inhibition is able to suppress the development of osimertinib resistance mediated by IFITM3.

Discussion

IFITM3, a small antiviral membrane protein whose expression is upregulated by various cytokines [26–28], has previously been associated with tumor progression and treatment resistance [29–31]. However, its potential role in EGFR-TKI resistance has been unknown. We have now shown that IFITM3 activates the PI3K-AKT signaling pathway through interaction with MET and thereby contributes to the development of resistance to osimertinib. IFITM3 expression in cancer cells is upregulated by cytokines derived from cells in the TME as well as from cancer cells themselves in response to osimertinib treatment. Through its interaction with MET, IFITM3 induces persistent AKT phosphorylation, even in the presence of osimertinib, thereby promoting cancer cell survival (Fig. 7).

Previous studies based on next-generation sequencing for analysis of genetic alterations in tumor specimens obtained after the development of EGFR-TKI resistance have identified resistance mechanisms including secondary *EGFR* mutations and amplification of *MET* or *HER2* [5–8, 32]. However, resistance mechanisms have remained unknown for about half of all cases, indicative of a role for nongenetic factors, such as increased expression of specific genes or proteins such as cytokines. Although inflammatory cytokines, specific immune cell types, and cancer-associated fibroblasts have been implicated in EGFR-TKI resistance [33–36], detailed mechanisms by which they might interact with *EGFR*-mutated tumor cells have not been characterized for clinical specimens. Our RNA-seq analysis of clinical specimens of *EGFR*-mutant NSCLC identified *IFITM3* as the only gene that was significantly upregulated in patients with a short PFS (< 12 months) compared with a long PFS (>20 months) for osimertinib treatment. Spatial transcriptomics analysis further indicated that *IFITM3* expression in tumor cells was increased by inflammatory cytokines released predominantly from TME cells surrounding the tumor cells after osimertinib treatment. The interaction between TME and tumor cells may therefore promote

the survival of tumor cells through upregulation of IFITM3. Our approach thus has the potential to provide insight into resistance mechanisms that cannot be identified by conventional sequencing analysis for detection of genetic alterations.

We showed that inflammatory cytokines were also produced by tumor cells themselves in response to osimertinib treatment, consistent with previous observations [15, 17, 36, 37]. Given that inhibition of IL-6R or TNF-α suppressed the osimertinib-induced increase in *IFITM3* expression in NSCLC cell lines, this effect of osimertinib was likely dependent on cytokines produced by the cells rather than on EGFR blockade itself. In addition, our spatial transcriptomics analysis revealed heterogeneous *IFITM3* expression within individual tumor specimens, and neighborhood analysis showed no consistent differences in the surrounding cell populations between IFITM3-positive and IFITM3-negative tumor cells. These findings suggest that the observed heterogeneity in *IFITM3* expression may reflect variable responsiveness of tumor cells to cytokines or differences in cytokine production within the TME. Further research is needed to elucidate how cytokines promote IFITM3 expression and how signaling heterogeneity arises within tumors.

Whereas activation of the PI3K-AKT pathway has previously been identified as a mechanism of EGFR-TKI resistance [38–40], the precise mechanisms underlying such activation have been unclear. We have now shown that IFITM3-MET interaction activates the AKT pathway and thereby induces osimertinib resistance. Our results also show that inhibition of lipid rafts attenuated MET phosphorylation and restored sensitivity to osimertinib in IFITM3-overexpressing cells. Given that IFITM3 is thought to function as a scaffold within lipid rafts and to activate B cell receptor signaling in B cell leukemia and lymphoma [25], it is possible that IFITM3 also acts as a scaffold to facilitate MET-PI3K pathway activation in lipid rafts of *EGFR*-mutant NSCLC cells. In addition, given that enhanced activity of the EGFR signaling pathway has been shown to activate the JAK-STAT and IRF signaling pathways [41, 42], both of which are known to upregulate IFITM3 [43–45], IFITM3 may play a key role in supporting the survival of tumor cells with *EGFR* mutations.

MET pathway activation is a well-characterized mechanism of acquired resistance to EGFR-TKI treatment [46, 47], with *MET* amplification having been identified in ~ 15% of cases of acquired resistance to osimertinib [48–50]. Preclinical and clinical studies have suggested that combination treatment with an EGFR-TKI and MET inhibitor is a promising strategy to overcome MET-driven resistance to EGFR-TKIs [51–55]. We have now shown that MET pathway activation can also occur through IFITM3 interaction with MET as a result of cytokine stimulation during osimertinib treatment, resulting in the development of resistance to osimertinib. We further showed that the combination of osimertinib and a MET inhibitor suppressed the MET-AKT signaling pathway and prevented the development of osimertinib resistance. Our findings highlight the potential of combined treatment with EGFR-TKIs and MET inhibitors not only to restore TKI sensitivity in *EGFR*-mutant NSCLC patients with acquired resistance to these drugs but also to prevent the development of such resistance in treatment-naïve patients. Indeed, the addition of the bispecific antibody amivantamab, which targets both EGFR and MET, to EGFR-TKI therapy was shown to improve PFS in patients with *EGFR* mutation–positive NSCLC [56].

Our study has several limitations. First, the proposed interaction between TME and tumor cells was not validated with in vivo models. Studies with humanized mouse models and patient-derived xenografts or cancer organoids may provide insight into such interaction and further corroborate our findings. Second, the potential association between increased IFITM3 expression and known acquired genetic alterations linked to osimertinib resistance was not assessed. Third, although we showed that IFITM3 expression increases in association with the development of resistance to osimertinib by IHC and spatial transcriptomics analysis of clinical specimens, the small number of matched patient samples limits the generalizability of these findings. Further large-cohort studies are needed to determine whether IFITM3 upregulation is associated with specific resistance mechanisms and to elucidate the detailed interactions between the TME and tumor cells.

Conclusions

In conclusion, we have identified upregulation of IFITM3 by cytokines derived from the TME or tumor cells themselves during osimertinib treatment as a previously unrecognized mechanism of acquired resistance to this drug. Targeting the IFITM3-MET axis offers a promising therapeutic strategy to improve treatment outcomes and to overcome IFITM3-mediated resistance to osimertinib in individuals with *EGFR*-mutant NSCLC.

Supplementary Information

The online version contains supplementary material available at https://doi.org/10.1186/s12943-025-02493-6.

Supplementary Material 1

Supplementary Material 2

Acknowledgements

We thank CyberomiX (Kyoto, Japan) for assistance with RNA-seq analysis; Terumi Ikenaga and the Research Support Center, Research Center for Human Disease Modeling, Kyushu University Graduate School of Medical Sciences,

for technical assistance; and the Laboratory for Technical Support (Medical Institute of Bioregulation, Kyushu University) for performing LC-MS/MS analysis.

Authors' contributions

Conceptualization: R.I. and E.I. Methodology: R.I., E.I., A.S., H.K., S. Mizusaki, and S.N. Investigation: R.I., E.I., A.S., S. Mizusaki, S.N., Y.M., Y.I., M.H., T.H., Y.T.-K., H.T., T.N., N.N., Y.K., S.K., and S. Mashimoto. Writing–original draft: R.I. and E.I. Writing–review and editing: R.I., E.I, Y.Y., D.S., K.O., K.T., and I.O. Funding acquisition: R.I., E.I., and I.O. Supervision: E.I., Y.O., and I.O.

Funding

This research was funded by the Japan Agency for Medical Research and Development (25lk0221207h0001), the Kakihara Foundation, the Kaibara Morikazu Medical Science Promotion Foundation, and The Shinnihon Foundation of Advanced Medical Treatment Research.

Data availability

All RNA-seq analysis data sets for clinical tumor specimens and NSCLC cell lines have been deposited, and processed values and complete gene lists are available, at GEO (http://www.ncbi.nlm.nih.gov/geo) under GEO series IDs GSE289619 and GSE289383, respectively. Spatial transcriptome analysis data sets have also been deposited and are available at GEO under GSE288758 and GSE301973. LC-MS/MS data sets have been deposited at Japan Proteome Standard Repository/Database (https://jpostdb.org) with the data set identifier JPST003605.

Declarations

Ethics approval and consent to participate

The analysis of clinical specimens in this study was approved by the ethics committee of Kyushu University Hospital (approval no. 23220-00; approval date, 6 October 2023) and was performed in accordance with the Declaration of Helsinki (as revised in 2013). Informed consent was obtained from the participating patients. Animal experiments were approved by the Kyushu University Animal Experiment Committee (approval no. A24-314-0) and were performed in accordance with Kyushu University Animal Experiment Regulations, related laws and regulations, and ARRIVE (Animal Research: Reporting of In Vivo Experiments) guidelines.

Consent for publication

Not applicable.

Competing interests

E.I. has received honoraria from AstraZeneca and Chugai Pharmaceutical. Y.T.-K. has received personal fees from Bristol-Myers Squibb, Taiho Pharmaceutical, Chugai Pharmaceutical, AstraZeneca, Kyowa Hakko Kirin, MSD, Ono Pharmaceutical, and Takeda Pharmaceutical outside the submitted work. D.S. has received honoraria from Eli Lilly Japan K.K. Y.Y. has received honoraria from AstraZeneca. K.T. has received honoraria from Chugai Pharmaceutical, AstraZeneca, Ono Pharmaceutical, Bristol-Myers Squibb, Eli Lilly, Takeda Pharmaceutical, Novartis Pharma K.K., Merck Biopharma, Kyowa Kirin, Daiichi-Sankyo, Pfizer, Amgen, Janssen Pharmaceutical K.K., and MSD, and is an advisory board member for Pfizer and Novartis Pharma K.K. I.O. has received honoraria and research funding from Daiichi Sankyo, Chugai Pharmaceutical, Eli Lilly Japan K.K., AstraZeneca, Taiho Pharmaceutical, Boehringer Ingelheim, and Ono Pharmaceutical; honoraria from Takeda Pharmaceutical and Novartis Pharma K.K.; and research funding from Bristol-Meyers Squibb and MSD Oncology. All other authors declare no competing interests.

Author details

[1]Department of Respiratory Medicine, Graduate School of Medical Sciences, Kyushu University, 3-1-1 Maidashi, Higashi-ku, Fukuoka 812-8582, Japan
[2]Department of Anatomic Pathology, Graduate School of Medical Sciences, Kyushu University, Fukuoka, Japan
[3]Department of Respiratory Medicine, Community Health Care Organization, Kyushu Hospital, Kitakyushu, Japan
[4]Department of Respiratory Medicine, Kitakyushu Municipal Medical Center, Kitakyushu, Japan
[5]Department of Respiratory Medicine, National Hospital Organization Fukuoka Higashi Medical Center, Koga, Japan
[6]Department of Respiratory Medicine, Saiseikai Fukuoka General Hospital, Fukuoka, Japan
[7]Department of Respiratory Medicine, Japanese Red Cross Fukuoka Hospital, Fukuoka, Japan
[8]Department of Respiratory Medicine, Kyushu Central Hospital, Fukuoka, Japan
[9]Department of Respiratory Medicine, St. Mary's Hospital, Kurume, Japan
[10]Department of Respiratory Medicine, Steel Memorial Yawata Hospital, Kitakyushu, Japan
[11]Department of Pulmonary Medicine, Graduate School of Medical and Dental Sciences, Kagoshima University, Kagoshima, Japan

Received: 25 February 2025 / Accepted: 1 October 2025
Published online: 28 October 2025

References

1. Sung H, Ferlay J, Siegel RL, Laversanne M, Soerjomataram I, Jemal A, et al. Global cancer statistics 2020: GLOBOCAN estimates of incidence and mortality worldwide for 36 cancers in 185 countries. CA Cancer J Clin. 2021;71:209–49.
2. Kobayashi Y, Mitsudomi T. Not all epidermal growth factor receptor mutations in lung cancer are created equal: perspectives for individualized treatment strategy. Cancer Sci. 2016;107:1179–86.
3. Gazdar A. Activating and resistance mutations of EGFR in non-small-cell lung cancer: role in clinical response to EGFR tyrosine kinase inhibitors. Oncogene. 2009;28:S24–31.
4. Soria J-C, Ohe Y, Vansteenkiste J, Reungwetwattana T, Chewaskulyong B, Lee KH, et al. Osimertinib in untreated EGFR-mutated advanced non–small-cell lung cancer. N Engl J Med. 2018;378:113–25.
5. Planchard D, Loriot Y, Andre F, Gobert A, Auger N, Lacroix L, et al. EGFR-independent mechanisms of acquired resistance to AZD9291 in EGFR T790M-positive NSCLC patients. Ann Oncol. 2015;26:2073–8.
6. Taniguchi H, Yamada T, Wang R, Tanimura K, Adachi Y, Nishiyama A, et al. AXL confers intrinsic resistance to osimertinib and advances the emergence of tolerant cells. Nat Commun. 2019;10:259.
7. Ho CC, Liao WY, Lin CA, Shih JY, Yu CJ, Yang JC. Acquired BRAF V600E mutation as resistant mechanism after treatment with osimertinib. J Thorac Oncol. 2017;12:567–72.
8. Piper-Vallillo AJ, Sequist LV, Piotrowska Z. Emerging treatment paradigms for EGFR-Mutant lung cancers progressing on osimertinib: A review. J Clin Oncol. 2020;38:2926–36.
9. Leonetti A, Sharma S, Minari R, Perego P, Giovannetti E, Tiseo M. Resistance mechanisms to osimertinib in EGFR-mutated non-small cell lung cancer. Br J Cancer. 2019;121:725–37.
10. Moghal N, Li Q, Stewart EL, Navab R, Mikubo M, D'Arcangelo E, et al. Single-cell analysis reveals transcriptomic features of drug-tolerant persisters and stromal adaptation in a patient-derived EGFR-mutated lung adenocarcinoma xenograft model. J Thorac Oncol. 2023;18:499–515.
11. Sun Y, Dong Y, Liu X, Zhang Y, Bai H, Duan J, et al. Blockade of STAT3/IL-4 overcomes EGFR T790M-cis-L792F-induced resistance to osimertinib via suppressing M2 macrophages polarization. EBioMedicine. 2022;83:104200.
12. Huang J, Lan X, Wang T, Lu H, Cao M, Yan S, et al. Targeting the IL-1beta/EHD1/TUBB3 axis overcomes resistance to EGFR-TKI in NSCLC. Oncogene. 2020;39:1739–55.
13. Wan X, Xie B, Sun H, Gu W, Wang C, Deng Q, et al. Exosomes derived from M2 type tumor-associated macrophages promote osimertinib resistance in non-small cell lung cancer through MSTRG.292666.16-miR-6836-5p-MAPK8IP3 axis. Cancer Cell Int. 2022;22:83.
14. Feng H, Cao B, Peng X, Wei Q. Cancer-associated fibroblasts strengthen cell proliferation and EGFR TKIs resistance through aryl hydrocarbon receptor dependent signals in non-small cell lung cancer. BMC Cancer. 2022;22:764.
15. Gong K, Guo G, Gerber DE, Gao B, Peyton M, Huang C, et al. TNF-driven adaptive response mediates resistance to EGFR inhibition in lung cancer. J Clin Invest. 2018;128:2500–18.
16. Gong K, Guo G, Panchani N, Bender ME, Gerber DE, Minna JD, et al. EGFR inhibition triggers an adaptive response by co-opting antiviral signaling pathways in lung cancer. Nat Cancer. 2020;1:394–409.

17. Ibusuki R, Iwama E, Shimauchi A, Tsutsumi H, Yoneshima Y, Tanaka K, Okamoto I. TP53 gain-of-function mutations promote osimertinib resistance via TNF-alpha-NF-kappaB signaling in EGFR-mutated lung cancer. NPJ Precis Oncol. 2024;8:60.
18. Patel SA, Nilsson MB, Yang Y, Le X, Tran HT, Elamin YY, et al. IL6 mediates suppression of T- and NK-cell function in EMT-associated TKI-resistant EGFR-mutant NSCLC. Clin Cancer Res. 2023;29:1292–304.
19. Ibusuki R, Yoneshima Y, Hashisako M, Matsuo N, Harada T, Tsuchiya-Kawano Y, et al. Association of thyroid transcription factor-1 (TTF-1) expression with efficacy of PD-1/PD-L1 inhibitors plus pemetrexed and platinum chemotherapy in advanced non-squamous non-small cell lung cancer. Transl Lung Cancer Res. 2022;11:2208–15.
20. Zhou Y, Zhou B, Pache L, Chang M, Khodabakhshi AH, Tanaseichuk O, et al. Metascape provides a biologist-oriented resource for the analysis of systems-level datasets. Nat Commun. 2019;10:1523.
21. Nakamura S, Shibahara D, Tanaka K, Kishikawa Y, Hashisako M, Nakatomi K, Nakagaki N, Kohno M, Azuma K, Ibusuki R et al. Spatial dynamics of the tumor microenvironment in emerging resistance to targeted therapy in EGFR-mutated NSCLC. Preprint at https://www.biorxivorg/content/101101/202502 10637543v1 .2025.
22. Ghandi M, Huang FW, Jane-Valbuena J, Kryukov GV, Lo CC, McDonald ER 3rd, Barretina J, Gelfand ET, Bielski CM, Li H, et al. Next-generation characterization of the cancer cell line encyclopedia. Nature. 2019;569:503–8.
23. Bailey CC, Huang I-C, Kam C, Farzan M. Ifitm3 limits the severity of acute influenza in mice. PLoS Pathog. 2012. https://doi.org/10.1371/journal.ppat.1002909.
24. Friedman RL, Manly SP, McMahon M, Kerr IM, Stark GR. Transcriptional and posttranscriptional regulation of interferon-induced gene expression in human cells. Cell. 1984;38:745–55.
25. Lee J, Robinson ME, Ma N, Artadji D, Ahmed MA, Xiao G, et al. IFITM3 functions as a PIP3 scaffold to amplify PI3K signalling in B cells. Nature. 2020;588:491–7.
26. Everitt AR, Clare S, Pertel T, John SP, Wash RS, Smith SE, et al. IFITM3 restricts the morbidity and mortality associated with influenza. Nature. 2012;484:519–23.
27. Poddar S, Hyde JL, Gorman MJ, Farzan M, Diamond MS. The Interferon-Stimulated gene IFITM3 restricts infection and pathogenesis of arthritogenic and encephalitic alphaviruses. J Virol. 2016;90:8780–94.
28. Hur JY, Frost GR, Wu X, Crump C, Pan SJ, Wong E, Barros M, Li T, Nie P, Zhai Y, et al. The innate immunity protein IFITM3 modulates gamma-secretase in alzheimer's disease. Nature. 2020;586:735–40.
29. Xiong Z, Xu X, Zhang Y, Ma C, Hou C, You Z, et al. IFITM3 promotes glioblastoma stem cell-mediated angiogenesis via regulating JAK/STAT3/bFGF signaling pathway. Cell Death Dis. 2024;15:45.
30. Liu X, Chen L, Fan Y, Hong Y, Yang X, Li Y, Lu J, Lv J, Pan X, Qu F, et al. IFITM3 promotes bone metastasis of prostate cancer cells by mediating activation of the TGF-beta signaling pathway. Cell Death Dis. 2019;10:517.
31. Chu P-Y, Huang W-C, Tung S-L, Tsai C-Y, Chen CJ, Liu Y-C, et al. IFITM3 promotes malignant progression, cancer stemness and chemoresistance of gastric cancer by targeting MET/AKT/FOXO3/c-MYC axis. Cell Biosci. 2022;12:124.
32. Wu S-G, Shih J-Y. Management of acquired resistance to EGFR TKI–targeted therapy in advanced non-small cell lung cancer. Mol Cancer. 2018;17:1–14.
33. Wang S, Rong R, Yang DM, Fujimoto J, Bishop JA, Yan S, et al. Features of tumor-microenvironment images predict targeted therapy survival benefit in patients with EGFR-mutant lung cancer. J Clin Invest. 2023. https://doi.org/10.1172/JCI160330.
34. Han R, Guo H, Shi J, Wang H, Zhao S, Jia Y, Liu X, Li J, Cheng L, Zhao C, et al. Tumour microenvironment changes after osimertinib treatment resistance in non-small cell lung cancer. Eur J Cancer. 2023;189:112919.
35. Nilsson MB, Sun H, Diao L, Tong P, Liu D, Li L, et al. Stress hormones promote EGFR inhibitor resistance in NSCLC: implications for combinations with β-blockers. Sci Transl Med. 2017;9:eaao4307.
36. Li L, Han R, Xiao H, Lin C, Wang Y, Liu H, et al. Metformin sensitizes EGFR-TKI–resistant human lung cancer cells *in vitro* and *in vivo* through inhibition of IL-6 signaling and EMT reversal. Clin Cancer Res. 2014;20:2714–26.
37. Yao Z, Fenoglio S, Gao DC, Camiolo M, Stiles B, Lindsted T, et al. TGF-β IL-6 axis mediates selective and adaptive mechanisms of resistance to molecular targeted therapy in lung cancer. Proc Natl Acad Sci U S A. 2010;107:15535–40.
38. Jacobsen K, Bertran-Alamillo J, Molina MA, Teixido C, Karachaliou N, Pedersen MH, Castellvi J, Garzon M, Codony-Servat C, Codony-Servat J, et al. Convergent Akt activation drives acquired EGFR inhibitor resistance in lung cancer. Nat Commun. 2017;8:410.
39. Kim TM, Song A, Kim D-W, Kim S, Ahn Y-O, Keam B, et al. Mechanisms of acquired resistance to AZD9291: a mutation-selective, irreversible EGFR inhibitor. J Thorac Oncol. 2015;10:1736–44.
40. Terp MG, Jacobsen K, Molina MA, Karachaliou N, Beck HC, Bertran-Alamillo J, et al. Combined FGFR and Akt pathway inhibition abrogates growth of FGFR1 overexpressing EGFR-TKI-resistant NSCLC cells. NPJ Precis Oncol. 2021;5:65.
41. Yarden Y, Sliwkowski MX. Untangling the erbb signalling network. Nat Rev Mol Cell Biol. 2001;2:127–37.
42. Yamashita M, Chattopadhyay S, Fensterl V, Saikia P, Wetzel JL, Sen GC. Epidermal growth factor receptor is essential for Toll-like receptor 3 signaling. Sci Signal. 2012;5:ra50–50.
43. Honda K, Taniguchi T. IRFs: master regulators of signalling by Toll-like receptors and cytosolic pattern-recognition receptors. Nat Rev Immunol. 2006;6:644–58.
44. Lewin AR, Reid LE, McMAHON M, Stark GR, Kerr IM. Molecular analysis of a human interferon-inducible gene family. Eur J Biochem. 1991;199:417–23.
45. Schneider WM, Chevillotte MD, Rice CM. Interferon-stimulated genes: a complex web of host defenses. Annu Rev Immunol. 2014;32:513–45.
46. Engelman JA, Zejnullahu K, Mitsudomi T, Song Y, Hyland C, Park JO, et al. MET amplification leads to gefitinib resistance in lung cancer by activating ERBB3 signaling. Science. 2007;316:1039–43.
47. Yano S, Wang W, Li Q, Matsumoto K, Sakurama H, Nakamura T, et al. Hepatocyte growth factor induces gefitinib resistance of lung adenocarcinoma with epidermal growth factor receptor–activating mutations. Cancer Res. 2008;68:9479–87.
48. Yu HA, Arcila ME, Rekhtman N, Sima CS, Zakowski MF, Pao W, et al. Analysis of tumor specimens at the time of acquired resistance to EGFR-TKI therapy in 155 patients with EGFR-mutant lung cancers. Clin Cancer Res. 2013;19:2240–7.
49. Leonetti A, Verze M, Minari R, Perrone F, Gnetti L, Bordi P, et al. Resistance to osimertinib in advanced EGFR-mutated NSCLC: a prospective study of molecular genotyping on tissue and liquid biopsies. Br J Cancer. 2024;130:135–42.
50. Chmielecki J, Gray JE, Cheng Y, Ohe Y, Imamura F, Cho BC, et al. Candidate mechanisms of acquired resistance to first-line osimertinib in EGFR-mutated advanced non-small cell lung cancer. Nat Commun. 2023;14:1070.
51. Xu L, Kikuchi E, Xu C, Ebi H, Ercan D, Cheng KA, et al. Combined EGFR/MET or EGFR/HSP90 inhibition is effective in the treatment of lung cancers codriven by mutant EGFR containing T790M and MET. Cancer Res. 2012;72:3302–11.
52. Sequist LV, Han JY, Ahn MJ, Cho BC, Yu H, Kim SW, Yang JC, Lee JS, Su WC, Kowalski D, et al. Osimertinib plus Savolitinib in patients with EGFR mutation-positive, MET-amplified, non-small-cell lung cancer after progression on EGFR tyrosine kinase inhibitors: interim results from a multicentre, open-label, phase 1b study. Lancet Oncol. 2020;21:373–86.
53. York ER, Varella-Garcia M, Bang TJ, Aisner DL, Camidge DR. Tolerable and effective combination of full-dose Crizotinib and osimertinib targeting MET amplification sequentially emerging after T790M positivity in EGFR-mutant non-small cell lung cancer. J Thorac Oncol. 2017;12:e85–8.
54. Gainor JF, Niederst MJ, Lennerz JK, Dagogo-Jack I, Stevens S, Shaw AT, Sequist LV, Engelman JA: Dramatic Response to Combination Erlotinib and Crizotinib in a Patient with Advanced, EGFR-Mutant Lung Cancer Harboring De Novo MET Amplification. J Thorac Oncol 2016, 11:e83-85.
55. Piotrowska Z, Isozaki H, Lennerz JK, Gainor JF, Lennes IT, Zhu VW, Marcoux N, Banwait MK, Digumarthy SR, Su W: Landscape of acquired resistance to osimertinib in EGFR-mutant NSCLC and clinical validation of combined EGFR and RET inhibition with osimertinib and BLU-667 for acquired RET fusion. Cancer discovery 2018, 8:1529-1539.
56. Cho BC, Lu S, Felip E, Spira AI, Girard N, Lee JS, Lee SH, Ostapenko Y, Danchaivijitr P, Liu B, et al. Amivantamab plus Lazertinib in Previously Untreated EGFR-Mutated Advanced NSCLC. N Engl J Med. 2024;391:1486–98.

Publisher's Note